Available online at www.sciencedirect.com
SCIENCE DIRECT®
PERGAMON
International Journal of Heat and Mass Transfer 46 (2003) 3521–3528
International Journal of HEAT and MASS TRANSFER
www.elsevier.com/locate/ijhmt

Impingement heat transfer of a single thermal plume on the upper wall

Koichi Ichimiya [a,*], Toshihisa Abe [b]

[a] Department of Mechanical System Engineering, University of Yamanashi, Takeda-4, Kofu, Yamanashi 400-8511, Japan
[b] Suzuki Co. Ltd., Takatsukamachi-300, Hamamatsu, Shizuoka 432-91, Japan

Received 19 August 2002

Abstract

We present numerical calculations of the generation, growth and impingement of a thermal plume in a two-dimensional buoyancy induced flow. Numerical values are obtained for the aspect ratios $H/W = 1/4$, 3/8, 1/2, the Grashof numbers $Gr = 10^4$, 10^5, and the Prandtl number $Pr = 170$. Impingement heat transfer on the upper wall is evaluated at various times. Numerical results show that before a thermal plume impinges on the upper heated wall, the thermal conduction layer, which is the stable stratification, near the upper wall becomes thinner and the local heat transfer peaks. The local Nusselt number approaches the steady condition after the impingement of a thermal plume. Additionally, under certain conditions the stream function takes a symmetrical form of two ellipses.

1. Introduction

The heat transfer of the buoyancy-induced flow was performed in a half-infinite space or in a restricted space such as an enclosure. In the case of a half-infinite space, Pera and Gebhart [1] observed the basic behavior of a thermal plume from a point or line source, analyzed it using the stability theory, and presented the instability by non-symmetry. Gebhart et al. [2] optically measured the interaction of two thermal plumes for various plume intensities and pitches of two heat sources. They recognized the effects of the heat source and environmental wall in an unsteady flow. Nakagomi and Hirata [3] examined the diffusing mechanism of flow turbulence in a two-dimensional form and presented the effects of non-uniformity and the temperature gradient of a thermal plume in the flow direction. Recently, some environmental problems have emerged, for example, diffusions of warm exhausting water and smoke into the atmosphere or heat islands in cities. Noto [4] and Noto and Okamoto [5] measured the fluctuating phenomenon of a thermal plume from a line source in a wide space by the smoke wire method, and analyzed the fluctuating spectrum of fluid temperature. They showed that the frequency of the fluctuation was proportional to one third power of supplied heat. In the case of a restricted space, Lai et al. [6] presented the attenuation effect of a wall in their analysis and experiment on the behavior of a thermal plume induced by the weak buoyancy along a vertical plate. Audunson and Gebhart [7] analyzed the secondary flow along a vertical plate and concluded that non-linearity was the critical determinant between stable and unstable states. Reimann [8] described the effects of the distance and the attitude from a heat source to a thermal plume on temperature distribution and heat flow rate. Sparrow and Shamsundar [9] reported that the behavior of a thermal plume in a melted liquid between a heated wall and a solid wall depended on the Rayleigh number based on layer thickness as a characteristic length. Heya et al. [10] numerically analyzed the characteristics of a natural convective heat transfer in a partitioned enclosure. Akino et al. [11] visualized the local behavior in a vertical circular tube with heated upper wall and cold bottom wall by way of a

* Corresponding author. Tel./fax: +81-55-220-8434.
E-mail address: ichimiya@ccn.yamanashi.ac.jp (K. Ichimiya).

0017-9310/03/$ - see front matter © 2003 Elsevier Science Ltd. All rights reserved.
doi:10.1016/S0017-9310(03)00142-X

Nomenclature

a	thermal diffusivity of fluid	U, V	dimensionless velocity along X, Y ($=uh/v$, vh/v)
b	width of heated section	w	width of an enclosure
Gr	Grashof number $[=g\beta h^3(T_H - T_i)/v^2]$	W	dimensionless width of an enclosure $=w/h$
h	height of an enclosure	α	local heat transfer coefficient
H	dimensionless height $=h/h=1$	β	expansion coefficient
Nu	Nusselt number ($=\alpha h/\lambda = C/\Theta_{IE}$)	Θ	dimensionless temperature $[=(T - T_i)/(T_H - T_i)]$
Pr	Prandtl number ($=v/a$)	λ	thermal conductivity
q	heat flux	v	kinematic viscosity
Ra	Rayleigh number ($=Gr \cdot Pr$)	ρ	density
T	temperature	τ	dimensionless time ($=tv/h^2$)
T_H	heated wall temperature	ψ	stream function
T_i	initial fluid temperature	Ψ	dimensionless stream function ($=\psi/v$)
t	time from start of heating	ω	vorticity
x, y	coordinate in Fig. 1	Ω	dimensionless vorticity ($=\omega h^2/v$)
X, Y	dimensionless coordinate ($=x/h$, y/h)		
u, v	velocity along x, y		

thermosensitive liquid crystal suspension and made a model based on the behavior of a thermal plume and a thermal boundary layer. Goldstein and Volino [12] measured the onset of natural convection, the development and breakdown of the thermal conduction layer on a horizontal surface. Perterson and Bayazitoglu [13] examined the flow conditions in two types of transition occuring in the jet from nozzle to fully developed and from momentum to buoyancy dominated flow. Bastiaans et al. [14] studied experimentally natural convection flow of water induced by a small prismatic heat sources in a confined space. They found that in the transition region from laminar flow to turbulent flow, the inter-scale kinetic energy transfer possesses a relative large scale standard deviation. Barozzi and Callticelli [15] predicted numerically buoyancy induced circulation in a two-dimensional closed cavity with internal heat sources. They presented the stability limit for laminar flow. However, we have not found the impingement heat transfer characteristics of the buoyancy induced flow on the upper wall.

There are various problems involved in research of a thermal plume, as described above. We have not found an analysis of the unsteady heat flow of the buoyancy-induced jet of a thermal plume to an upper wall. The present study describes the numerical analysis of a two-dimensional unsteady heat transfer for the impingement of a thermal plume from a heat source on the bottom wall to the upper wall in an enclosure. In our analysis, we achieved results that contribute to the heat removal to an opposite plate or wall in a comparatively narrow space, namely, a compact heat exchanger, a heat-saving bath, or a room with floor heating.

2. Numerical analysis

Fig. 1 shows a two-dimensional space, whose height is h, width w, and the gravity works in the negative direction of x. The width b at the center of the horizontal wall is heated at a constant temperature T_H. An upper wall, on which a thermal plume impinges, is heated uniformly. The other walls are insulated thermally. Initial fluid temperature is T_i. The working fluid is Newtonian and incompressible. The physical properties are constant except for density. Boussinesq approximation is applied in the buoyancy term and thermal radiation is neglected.

Governing equations are arranged in dimensionless form introducing stream function ψ and vorticity ω. The followings are dimensionless definitions for the velocity components, length, time, vorticity, stream function, temperature, Grashof number and Prandtl number:

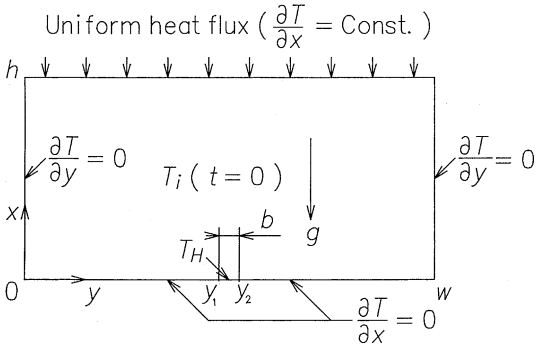

Fig. 1. Schematic diagram of two-dimensional domain.

$$U=\frac{uh}{v}\quad V=\frac{vh}{v}\quad X=\frac{x}{h}\quad Y=\frac{y}{h}\quad \tau=\frac{tv}{h^2}$$
$$\Omega=\frac{\omega h^2}{v}\quad \Psi=\frac{\psi}{v}\quad \Theta=\frac{(T-T_i)}{(T_H-T_i)} \tag{1}$$
$$Gr=\frac{g\beta h^3(T_H-T_i)}{v^2}\quad Pr=\frac{v}{a}$$

Dimensionless governing equations, initial conditions and boundary conditions are as follows:

Equations for fluid flow,

$$\frac{\partial^2\Psi}{\partial Y^2}+\frac{\partial^2\Psi}{\partial X^2}=-\Omega \tag{2}$$

$$\frac{\partial\Omega}{\partial\tau}+\left(\frac{\partial\Psi}{\partial Y}\frac{\partial\Omega}{\partial X}-\frac{\partial\Psi}{\partial X}\frac{\partial\Omega}{\partial Y}\right)=\left(\frac{\partial^2\Omega}{\partial Y^2}+\frac{\partial^2\Omega}{\partial X^2}\right)-Gr\frac{\partial\Theta}{\partial Y} \tag{3}$$

Equation for energy,

$$\frac{\partial\Theta}{\partial\tau}+\left(\frac{\partial\Psi}{\partial Y}\frac{\partial\Theta}{\partial X}-\frac{\partial\Psi}{\partial X}\frac{\partial\Theta}{\partial Y}\right)=\frac{1}{Pr}\left(\frac{\partial^2\Theta}{\partial Y^2}+\frac{\partial^2\Theta}{\partial X^2}\right) \tag{4}$$

Dimensionless initial conditions are:

$$\text{At } \tau=0,\quad \Psi=\Omega=\Theta=0. \tag{5}$$

Dimensionless boundary conditions are:

$$\begin{aligned}&\text{At } \tau>0,\\ &\Psi=0,\quad \partial\Theta/\partial X=0 \quad \text{at } X=0,\ 0\leqq Y\leqq Y_1,\ Y_2\leqq Y\leqq W\\ &\Psi=0,\quad \Theta=1 \quad \text{at } \underline{X}=0,\ Y_1\leqq Y\leqq Y_2\\ &\Psi=0,\quad \partial\Theta/\partial Y=0 \quad \text{at } 0\leqq X\leqq 1,\ Y=0,\ Y=W\\ &\Psi=0,\quad \partial\Theta/\partial X=C \quad \text{at } X=1,\ 0\leqq Y\leqq W\end{aligned} \tag{6}$$

where Y_1 and Y_2 denote the respective position of the left and right edge in the region with high temperature on the bottom wall. The system, is geometrically symmetrical. However, the computation was performed in the whole area because an unstable phenomenon is revealed. The constant number C is the heat flux coefficient on the upper wall defined as $qh/\{\lambda(T_H-T_i)\}$ and includes an enclosure height h. Therefore, in the present computation C was varied by the aspect ratio. Heat transfer on the upper wall, where a thermal plume impinged, was evaluated by the local Nusselt number Nu defined as follows:

$$Nu=\frac{\alpha h}{\lambda}=\frac{C}{\Theta_{IE}} \tag{7}$$

where Θ_{IE} is the dimensionless local temperature on the upper wall.

In numerical calculation, the alternating direction implicit (ADI) method was applied in the analysis of the dimensionless temperature Θ and vorticity Ω and the successive over-relaxation (SOR) method was used for the dimensionless stream function Ψ. Numerical accuracy of the calculation procedure was examined by conducting sensitivity tests and making comparisons with accepted results for natural convection. The sensitivity tests involved varying the spacings of the nodes and convergence criteria. The effect of the mesh size was evaluated previously for four sizes (ΔX, $\Delta Y=0.05$, 0.025, 0.01 and 0.005). There was no clear difference in dimensionless temperature and vorticity for (ΔX, $\Delta Y=0.01$ and 0.005). Therefore, the grid size (ΔX, $\Delta Y=0.01$) was determined. Ten meshes near the wall and twenty meshes near the heated section are half the size of the grid described above. The maximum number of the mesh was 20,000 grids. Central-difference and forward-difference expressions were utilized on the derivative with respect to X and Y and with respect to time τ, respectively. The two-step progress method was applied in the time step to stabilize the numerical solution, namely, the time step progress from n to $(n+1/2)$ and from $(n+1/2)$ to $(n+1)$. The dimensionless time step $\Delta\tau$ ranges from 10^{-3} to 2.8×10^{-6} depending on the numerical conditions. The criteria for convergence were employed for the maximum absolute difference, $|\Psi^{m+1}-\Psi^m|\leqq 5\times10^{-3}$. In addition, the heat transfer of natural convection on L-type heated surface was predicted by the same numerical procedure and the results agreed fairly well with experimental results [16].

Numerical conditions are as follows: aspect ratio $H/W=1/4$, 3/8, 1/2, Grashof number $Gr=10^4$, 10^5 (partly, 10^3), constant number $C=0.05$ for $H/W=1/4$, 0.075 for $H/W=3/8$, 0.1 for $H/W=1/2$, dimensionless heated wall width $b/h=0.2$ for $H/W=1/4$, 0.13 for $H/W=3/8$, and 0.1 for $W/H=1/2$. The working fluid is silicone oil, whose Prandtl number is 170, used for flow visualization by thermosensitive liquid crystal suspension.

3. Visualization by thermosensitive liquid crystal suspension

Visualization of a thermal plume corresponding to the numerical estimation was carried out by thermosensitive liquid crystal suspensions. The enclosure is 200-mm wide, 75-mm high and 100-mm breadth and the heated section is 10-mm wide at the center of the bottom wall. A weighted quantity of a liquid crystal powder 0.2 g/l was mixed into a solvent silicone oil to form a suspension. The powder particle size was about 50 μm. The powder floated in the solvent for several hours because the density was almost the same. The temperatures and flow were visualized simultaneously. The side walls of the enclosure were made of transparent acrylic plates. The upper wall was composed of stainless steel foil (20-μm thick), a thermosensitive liquid crystal sheet, and a transparent acrylic plate (10-mm thick) and

the temperature was visualized when a thermal plume impinged upon the upper wall. Thermosensitive liquid crystal is not appropriate for the measurement of rapid phenomena because its response is not clear. However, it is useful for temperature measurement in an almost steady state or slow phenomena. In the present experiment, the appropriate temperature range of the thermosensitive liquid crystal used is from 25 to 30 °C for suspension and from 28 to 35 °C for a sheet on the upper wall.

4. Results and discussion

4.1. Transient behavior of a thermal plume

Figs. 2 and 3 present the transient change of dimensionless temperature Θ and dimensionless stream function Ψ for $H/W = 3/8$ and $Gr = 10^4$ in the behavior of a thermal plume in an enclosure. At initial heating, a thermal conduction layer, which is a stable stratification, is generated on a horizontal surface, and a protuberance induced by buoyancy force also appears at the center for Rayleigh number $Ra_\delta = 10^3$ based on layer thickness δ as a characteristic length [17]. A thermal plume rises with a convex shape [Fig. 2(b) and (c)]. At $\tau = 3.2 \times 10^{-1}$ [Fig. 2(d)], a closed high-temperature region is separated, and a new high-temperature region is generated. The thermal conduction layer near the upper wall is pushed up as a thermal plume approaches the upper wall. At $\tau = 3.733 \times 10^{-1}$ [Fig. 2(e)], a thermal plume invades the thermal conduction layer and after the fluid, whose temperature is lower than the upper wall temperature, first impinges upon the upper wall, a higher temperature thermal plume follows. The shape of the higher-temperature plume is semi-circular [Fig. 2(d)] and flat. The shape affects the pushing effect of the thermal boundary layer. Fluid temperatures around the upper wall increase, and the high-temperature region extends to both side walls. The next thermal plume does not clearly affect the upper wall as the first plume does because the temperature near the upper wall becomes high. Fig. 3(a)–(f) shows the transient dimensionless stream functions around a thermal plume. The symmetrical recirculated flows are generated with the growth of thermal plumes and the center of the plume moves up and down or left

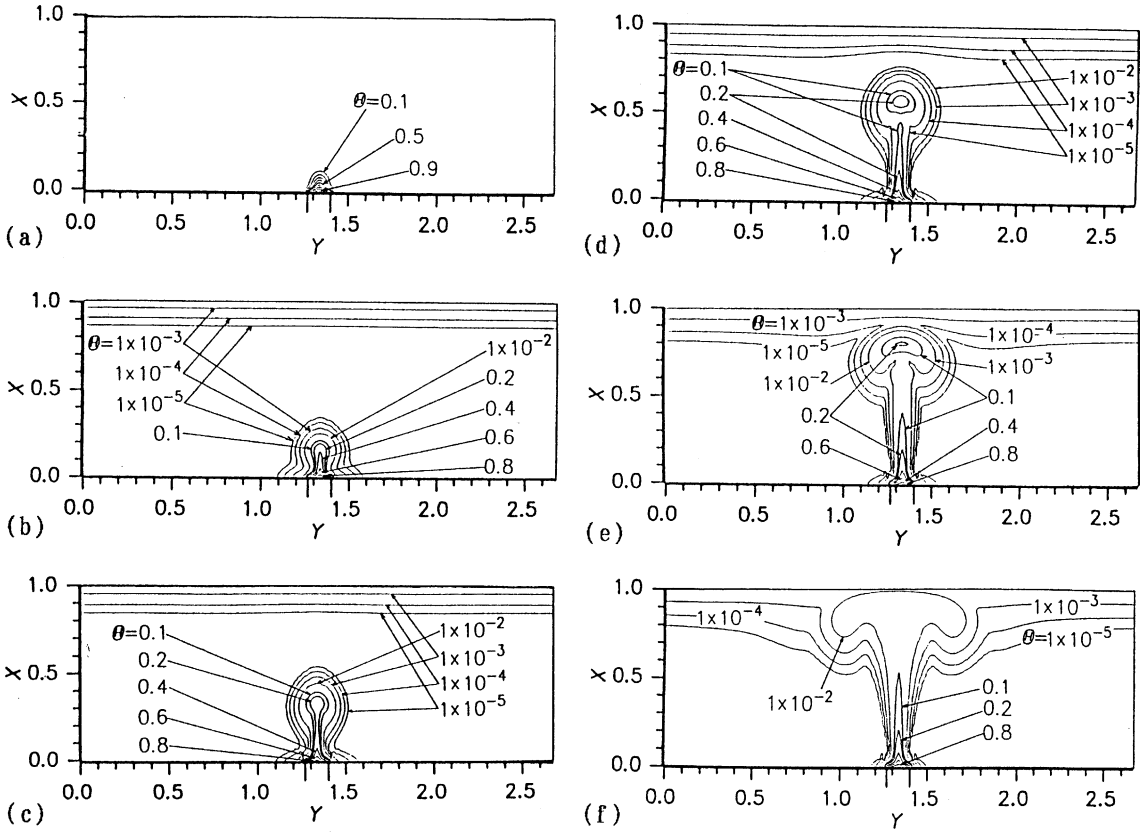

Fig. 2. Dimensionless temperature distribution Θ ($H/W = 3/8$, $Gr = 10^4$). (a) $\tau = 1.598 \times 10^{-1}$, (b) $\tau = 2.133 \times 10^{-1}$, (c) $\tau = 2.666 \times 10^{-1}$, (d) $\tau = 3.200 \times 10^{-1}$, (e) $\tau = 3.733 \times 10^{-1}$, (f) $\tau = 4.795 \times 10^{-1}$.

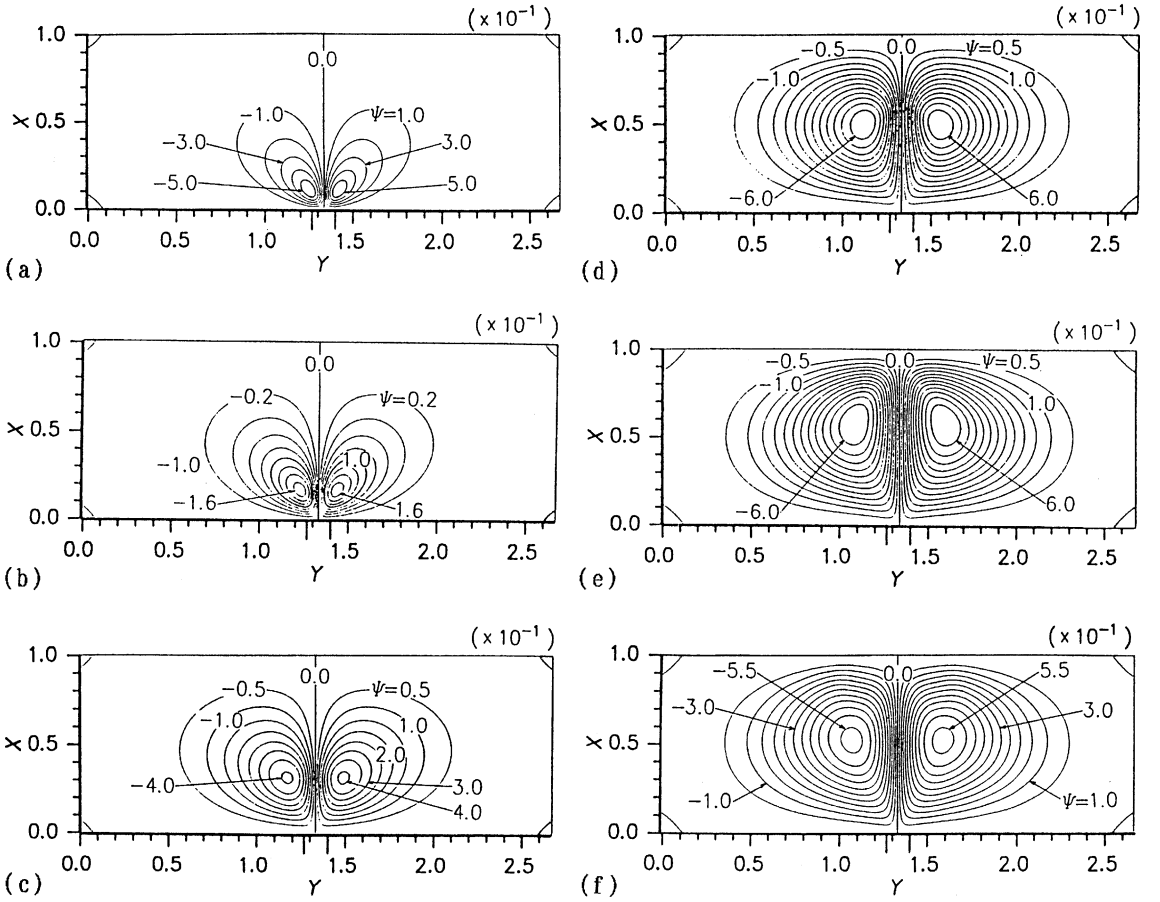

Fig. 3. Dimensionless stream function Ψ ($H/W = 3/8$, $Gr = 10^4$). (a) $\tau = 1.598 \times 10^{-1}$, (b) $\tau = 2.133 \times 10^{-1}$, (c) $\tau = 2.666 \times 10^{-1}$, (d) $\tau = 3.200 \times 10^{-1}$, (e) $\tau = 3.733 \times 10^{-1}$, (f) $\tau = 4.795 \times 10^{-1}$.

and right. Being close to the heated section, the shape of the iso-stream function is initially elliptic and convex to the outside. The center of the egg-like shapes moves to $X = 0.5$ at $\tau = 3.2 \times 10^{-1}$ and denotes a decrease in rising velocity. At $\tau = 3.733 \times 10^{-1}$, because a thermal plume approaches the upper wall, the shape of the stream function is elliptic and convex to the inside. The center moves to $X = 0.6$, and does not rise after that.

At $\tau = 8 \times 10^{-2}$ for $Gr = 10^5$ [Fig. 4(a)], the thermal plume rises up to $X = 0.65$, and the rising velocity is $\sqrt{10}$ times higher than that of $Gr = 10^4$. The shape of the isothermal lines is upwardly and downwardly convex. It affects the pushing effect of a thermal conduction layer on the upper wall and the local heat transfer characteristics on the upper wall. The center of a dimensionless stream function [Fig. 4(b)] approaches the

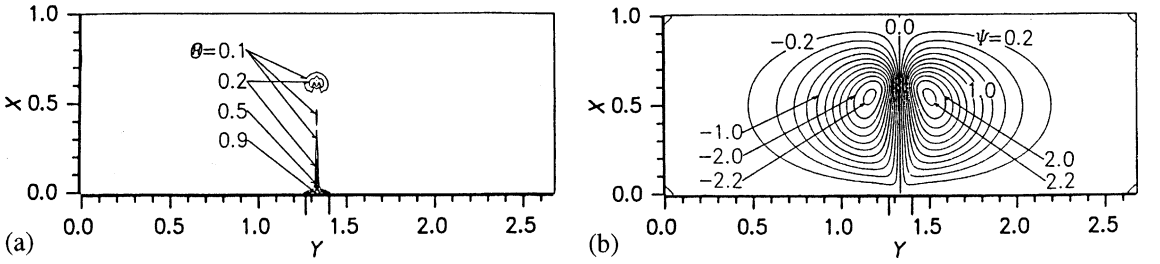

Fig. 4. Thermal plume ($Gr = 10^5$, $H/W = 3/8$, $\tau = 8 \times 10^{-2}$). (a) Dimensionless temperature Θ. (b) Dimensionless stream function Ψ.

upper wall in the shape of an elliptic convexity to the left and right sides.

4.2. Heat transfer on the upper wall

Fig. 5(a) and (b) shows the local Nusselt number on the upper wall at the impingement of thermal plumes as a parameter of dimensionless time. The abscissa is the horizontal distance Y, and the ordinate is the local Nusselt number. At $\tau = 3.600 \times 10^{-1}$ in Fig. 5(a) which corresponds to Figs. 2 and 3, Nu peaks at the center. As shown in Fig. 2(e), the low temperature layer pushed by the plume impinges upon the upper wall, which is cooled instantaneously. That is why the heat transfer is higher than its surroundings. In the next step, the high-temperature layer impinges, and the local heat transfer takes a minimum value. The high-temperature region expands in the Y direction. This expansion represents the size of thermal plumes. When the upper wall temperature approaches T_H, the dimensionless temperature Θ_{IE} becomes 1. As a result, Nu approaches the dimensionless heat flux C. For $Gr = 10^5$, four peaks of Nu appear at $\tau = 1.066 \times 10^{-1}$ and two peaks at $\tau = 1.322 \times 10^{-1}$. This depends on the pushing effect of the low temperature thermal conduction layer due to the shape change in the thermal plume, as shown in Fig. 4(a). Particularly at $\tau = 1.066 \times 10^{-1}$, the distribution of Nusselt number is asymmetrical for the center of heated plate. This peak is instantaneously two orders higher than the local Nusselt number around it. For comparatively high Grashof numbers, the local Nusselt number may become unstable and be asymmetrical at a large temperature difference between the initial plume and the surrounding fluid. The instability may be generated because the Grashof number $Gr = 10^5$ corresponds to the Rayleigh number $Ra = 1.7 \times 10^7$. However, this asymmetry may be an error in the numerical computation. In order to determine whether or not this is an error, the computation was performed again for a half-size grid near the impingement surface with many iterations. As the result, there was no remarkable difference in the numerical results and such an asymmetry was generated. Therefore, this asymmetry appears as an unstable phenomenon. For $H/W = 3/8$ and $Gr = 10^5$, the color distributions of the thermosensitive liquid crystal suspension and of the sheet on the upper wall at the impingement of the thermal plume at $\tau \fallingdotseq 10$ are presented in Fig. 6(a) and (b), respectively. Fig. 6(a) shows simultaneously the temperature and flow visualization. Color yellow–green means relatively lower temperature to color blue. According to Fig. 6(a), the rising flow in the central section and the recirculated flow to both sides can be seen. On the other hand, according to the color distribution on the upper wall [Fig. 6(b)], a thermal plume impinges with a stripe-like pattern along the breadth. This shows the three-dimensionality of the phenomenon and we

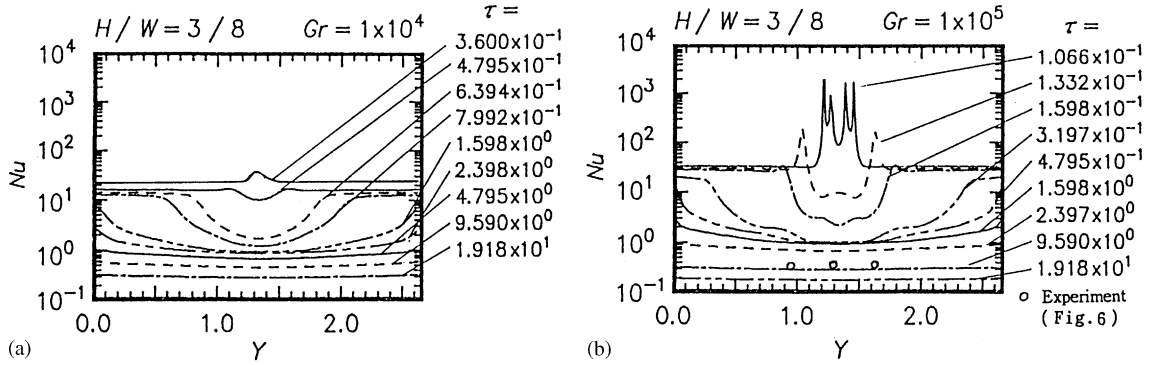

Fig. 5. Local Nusselt number ($H/W = 3/8$). (a) $Gr = 10^4$, (b) $Gr = 10^5$.

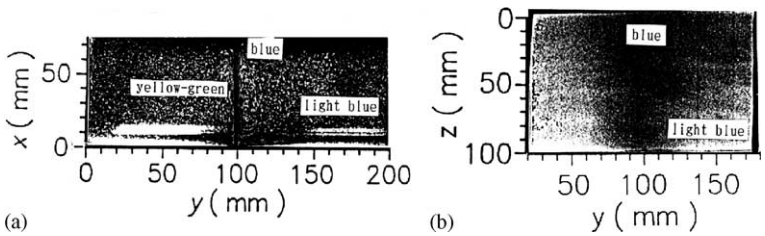

Fig. 6. Color distribution ($H/W = 3/8$, $Gr \fallingdotseq 10^5$, $\tau \fallingdotseq 10$). (a) Thermal plume. (b) Color distribution on upper wall.

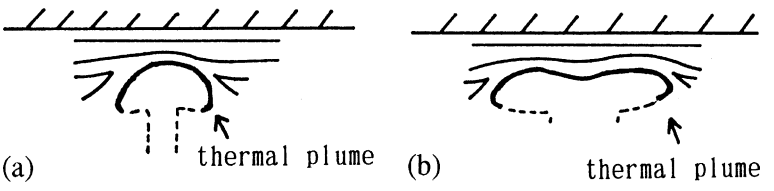

Fig. 7. Impingement model of thermal plume. (a) Semi-circular type, (b) Uneven type.

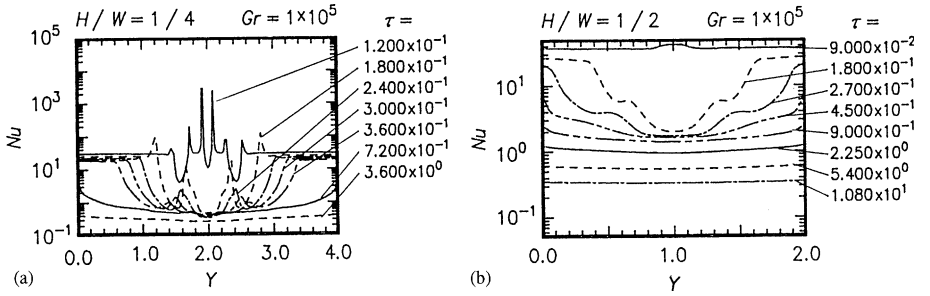

Fig. 8. Local Nusselt number Nu ($Gr = 10^5$). (a) $H/W = 1/4$, (b) $H/W = 1/2$.

believe that it should be studied in detail. The experimental values of Nusselt numbers on the upper wall are presented by the symbol ○ in Fig. 5(b). The side walls are assumed to be insulated thermally in our numerical calculation, but the insulation was not perfect in the experiment. Therefore, there is some difference between the experimental and numerical values due to a heat loss by thermal conduction. Consequently, the characteristics of the local Nusselt number distributions were divided into three, namely, the protrusive distribution with one or several peaks, the hollow one with the minimum and the flat one. These transient change depends on the Grashof number Gr and the aspect ratio H/W.

Fig. 7(a) and (b) shows a model of the thermal plume at its impingement. At low Gr number and high H/W, a single peak of the Nusselt number can be found in a shape with a semi-circular top [Fig. 7(a)]. The stabilized thermal conduction layer affects the shape. On the other hand, at high Gr number and low H/W, an uneven shape of a thermal plume is a cause of several peaks of the Nusselt number [Fig. 7(b)].

Fig. 8(a) and (b) shows the effect of aspect ratio H/W on the local Nusselt number. In the case of $H/W = 1/4$ [Fig. 8(a)], the heat does not diffuse much into the surroundings until a high-temperature plume approaches the upper wall. This is due to the fact that the height of the vessel becomes relatively lower than that of $H/W = 3/8$. The maximum and minimum values of Nusselt number appear clearly because of the high temperature gradient at the upper wall, and the distribution at $\tau = 0.12$ is asymmetrical. After that, two peaks are found symmetrically at the center of the heated section. On the other hand, for $H/W = 1/2$ [Fig. 8(b)], the approaching velocity of a thermal plume to the upper wall decreases, and thermal diffusion increases because the height becomes relatively greater than $H/W = 3/8$. Therefore, the local Nusselt number does not change remarkably along the width or with time.

The minimum Nusselt number Numin for $H/W = 3/8$ is presented in Fig. 9 as a parameter of Gr. In the case of $Gr = 10^3$, after a thermal plume impinges on the upper wall, Nu decreases rapidly with the generation of a high temperature layer ranging from $\tau = 0.1$

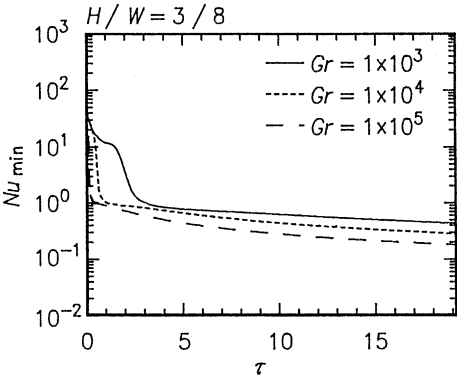

Fig. 9. Transient variation of minimum Nusselt number Numin ($H/W = 3/8$).

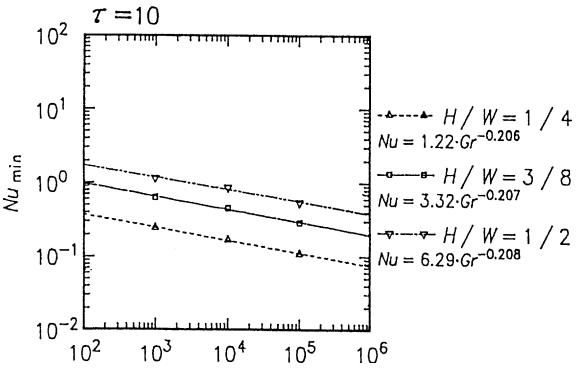

Fig. 10. Relationship between Numin and *Gr*.

to 0.15 and then stabilizes. In the case of $Gr = 10^3$, *Nu* moves to a stable region via two steps, namely, the generation of a high-temperature layer due to the impingement of the first thermal plume and the impingement of the next thermal plume upon the thin layer after the diffusion.

Fig. 10 shows the relationship between Numin and *Gr* in a stable region at $\tau = 10$. The abscissa is *Gr* and the ordinate Numin. Fig. 10 denotes that Numin depends on $Gr^{-0.2}$ for each H/W. Clifton and Chapman [18] numerically examined the heat transfer for the case in which fluid impinges on a cold plate facing upwards, and they obtained the relationship $Nu \sim Gr^{1/5}$. These indicate that even if the plate is heated or cooled, in the impingement heat transfer by buoyancy-induced flow, *Nu* depends on the absolute index 1/5 of *Gr*.

5. Conclusions

In a rectangular enclosure heated locally, the growth, separation, rise and impingement process of a thermal plume were analyzed numerically in an unsteady condition, and the impingement heat transfer on the upper wall was evaluated. A thermal plume composes of a high temperature layer depending on Grashof number *Gr*, pushes up the low temperature thermal conduction layer around the upper wall and impinges upon the upper wall. Therefore, the local Nusselt number produces a complicated distribution with peaks or minimums depending on the shape of the top of a thermal plume and moves to a stable region in the direction of the width. The impingement model of a thermal plume is classified into a semi-circular type and an uneven type. The minimum Nusselt number Numin in a stable region depends on $Gr^{-0.2}$.

References

[1] L. Pera, B. Gebhart, On the stability of laminar plumes: some numerical solutions and experiments, Int. J. Heat Mass Transfer 14 (1971) 975–983.
[2] B. Gebhart, H. Shaukatullah, L. Pera, The interaction of unequal laminar plane plumes, Int. J. Heat Mass Transfer 19 (1976) 751–756.
[3] H. Nakagomi, M. Hirata, Turbulent diffusion mechanism of two-dimensional thermal plume, Trans. JSME (ser. B) 46 (410) (1980) 2023–2032.
[4] K. Noto, Swaying motion in thermal plume above a horizontal line heat source, J. Thermophys. Heat Transfer 3 (4) (1989) 428–434.
[5] K. Noto, H. Okamoto, Thermal plume from a heated source in thermally stable stratified air: fundamental characteristics of heat island phenomenon, Energy Building 15/16 (1990/91) 183–190.
[6] M.C. Lai, S.M. Jeng, G.M. Faeth, Structure of turbulent adiabatic wall plumes, Trans. ASME (ser. C) 108 (1986) 834–927.
[7] T. Audunson, B. Gebhart, Secondary mean motions arising in a buoyancy induced flow, Int. J. Heat Mass Transfer 19 (1976) 737–750.
[8] J. Reimann, Experimental investigation of free convection flow from wires in the vicinity of phase interfaces, Int. J. Heat Mass Transfer 17 (1974) 1051–1061.
[9] E.M. Sparrow, N. Shamsundar, Convective instability in a melt layer heated from below, Trans. ASME (ser. C) 98 (1976) 88–94.
[10] N. Heya, M. Takeuchi, T. Kimura, Natural convection heat transfer in a partitioned enclosure (numerical analysis), Trans. JSME (ser. B) 50 (451) (1984) 724–731.
[11] N. Akino, T. Kunugi, Y. Shiina, M. Seki, Y. Okamoto, Natural convection in a horizontal silicone oil layer in a circular cylinder heated from below and cooled from above, Trans. JSME (ser. B) 55 (509) (1989) 152–158.
[12] R.J. Goldstein, R.J. Volino, Onset and development of natural convection above a suddenly heated horizontal surface, Trans. ASME (ser. C) 117 (1995) 808–821.
[13] J. Perterson, Y. Bayazitoglu, Measurement of velocity and turbulence in vertical axisymmetric isothermal and buoyant jets, Trans. ASME (ser. C) 114 (1992) 135–142.
[14] R.J.M. Bastiaans, C.C.M. Rindt, A.A. van Steenhoven, Experimental analysis of a confined transitional plume with respect to subgrid-scale modelling, Int. J. Heat Mass Transfer 41 (1998) 3989–4007.
[15] G.S. Barozzi, M.A. Corticelli, Natural convection in cavities containing internal sources, Heat Mass transfer 36 (2000) 473–480.
[16] K. Ichimiya, H. Takiguchi, Numerical analysis on unsteady natural convective heat transfer from L-type heated surface, J. SHASE 69 (1998) 75–84.
[17] J.S. Turner, Buoyancy Effects in Fluids, Cambridge University Press, London, 1973, pp. 226–230.
[18] J.V. Clifton, A.J. Chapman, Natural convection on a finite size horizontal plate, Int. J. Heat Mass Transfer 12 (1969) 1573–1584.